Two-Photon Dissociation Study of CS_2 Using Ion Imaging

Peter C. Samartzis and Theofanis N. Kitsopoulos*

Department of Chemistry, University of Crete and Institute of Electronic Structure and Laser, Foundation for Research and Technology-Hellas, 711 10 Heraklion-Crete, Greece

Received: January 29, 1997; In Final Form: April 3, 1997[⊗]

The $^1D_2$ and $^3P_{2,1,0}$ electronic states of the S-atom photofragments following the two-photon dissociation of cold CS_2 at 69399, 64893, 64496, 64320 cm^{-1}, respectively, are probed using ion imaging. From the S-atom photofragment translational energy distribution we conclude that CS is produced in both the $X^1\Sigma^+$ and $a^3\Pi$ electronic states with a branching ratio $CS(a^3\Pi) + S(^3P_2)/CS(X^1\Sigma^+) + S(^3P_2) = 0.22 \pm 0.05$ (at 64893 cm^{-1}), and 50% of the available energy is taken up by the CS internal degrees of freedom. By analyzing the photofragment angular distributions, we conclude that the excited electronic states involved in the photodissociation process are the Rydberg states with predissociation lifetimes estimated at ∼1 ps.

Introduction

Carbon disulfide belongs to a group of linear triatomic molecules with 16 valence electrons such as CO_2, ICN, OCS, and N_2O. The low-resolution absorption spectrum of this molecule, reported by Rabalais *et al.*,[1] consists of broad continua and sharp transitions to various Rydberg states. Numerous experimental studies[2−10] using a plethora of methods have tried to elucidate both the spectroscopy and the dynamics of this species. As this centrosymmetric molecule most probably cleaves along a CS bond, one would expect the photodissociation of CS_2 to be a fairly simple exercise in chemical dynamics. Yet, the intricate details such as the fine structure and energy partitioning amongst the photofragments remain unanswered.

The majority of photodissociation studies on CS_2 have been performed at 193 nm partly because the strongest feature in the CS_2 absorption spectrum lies within this energy region[1] and partly because of the facile production of this radiation *via* an ArF excimer laser. Although all experiments agreed that the processes taking place at this excitation energy (6.4 eV) are the following:

$$CS_2 \rightarrow CS(X^1\Sigma^+) + S(^3P)$$

$$\rightarrow CS(X^1\Sigma^+) + S(^1D)$$

discrepancies arose concerning the branching ratios amongst the two channels. The controversy was settled by Waller *et al.*[3] who used photofragment spectroscopy to conclude that this branching ratio is $S(^3P)/S(^1D) = 2.8 \pm 0.3$, *i.e.*, the spin-forbidden triplet channel is 3 times more probable than the singlet channel. Measurements of the angular distribution led to speculations concerning the excited state geometry and lifetime.

The previous experiment demonstrates the power of photofragment spectroscopy as means of elucidating both the dynamics and spectroscopy of excited states. For single photon excitation the symmetry selection rules limit the number of accessible final states, *e.g.*, as the symmetry of ground state CS_2 is *gerade*, only *ungerade* states can be accessed. Alternatively, in a two-photon excitation experiment, final states with *gerade* symmetry can be probed thus producing complementary information. Brewer *et al.*[11] first used two-photon excitation of CS_2 mostly as means of producing sulfur atoms which they studied using two-photon laser-induced fluorescence (LIF) and two-photon resonance-enhanced ionization. Fotakis *et al.*[12] reported multiphoton dissociation experiments at 248 nm while probing the dispersed fluorescence of the CS photofragments. Their observations were analyzed within the context of higher Rydberg states.

Hardwick *et al.*[13] used resonance-enhanced multiphoton ionization (REMPI) detection of the photofragments coupled with time-of-flight analysis to study the two-photon dissociation of CS_2 between 330 and 280 nm. The energetically allowed dissociation channels at these energies are the following:

$$CS_2 \longrightarrow CS(a^3\Pi) + S(^3P) \quad (1)$$

$$CS_2 \longrightarrow CS(X^1\Sigma^+) + S(^3P) \quad (2)$$

$$CS_2 \longrightarrow CS(X^1\Sigma^+) + S(^1D) \quad (3)$$

$$CS_2 \longrightarrow CS(X^1S^+) + S(^1S) \quad (4)$$

On the basis of their observations, they were able identify channel 1, but were unable to speculate on the importance of the other channels. Donaldson and co-workers[14] used LIF detection of the CS fragment following the photolysis of CS_2 at 308 nm and observed production of vibrationally hot $CS(X^1\Sigma^+)$. However, as the translational energy release was not measured, discrimination between reactions 2 and 3 was not possible. Kawasaki *et al.*[15,16] studied the two-photon dissociation of CS_2 from 288 to 310 nm by measuring the angular and speed distributions of the nascent S-atoms. Using REMPI they were able to unambiguously identify the spin−orbit electronic state of the sulfur photofragment, while from the translational energy distributions they concluded that all reaction channels (1−4) are active. From the measured photofragment angular distributions, anisotropy parameters were determined, but it was not possible to discriminate between reactions 1 and 2, as simultaneous monitoring of the CS and S-atom electronic state was not permitted in their experimental arrangement.

In this report we present our findings concerning the one-color two-photon excitation of cold CS_2 using the technique of ion imaging.[17] This method allows us to simultaneously probe both the translational energy release and angular distribution

* To whom all correspondence should be addressed: P.O. Box 1527, phone, ++30-81-391467; fax, ++30-81-391318; email, theo@luce.iesl.forth.gr.

⊗ Abstract published in *Advance ACS Abstracts,* July 1, 1997.

S1089-5639(97)00366-6 CCC: $14.00

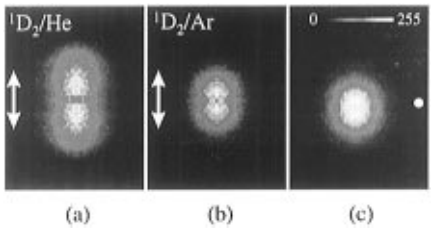

Figure 1. (a) Ion image for the $S(^1D_2)$ photofragment following the two-photon excitation of CS_2 seeded in a molecular beam of He, with the laser polarization parallel to the imaging plane (vertical double arrow). (b) Ion image for the $S(^1D_2)$ photofragment following the two-photon excitation of CS_2 seeded in a molecular beam of Ar, with the laser polarization parallel to the imaging plane (verticle double arrow). (c) Ion image for the $S(^1D_2)$ photofragment following the two-photon excitation of CS_2 seeded in a molecular beam of He, with the laser polarization perpendicular to the imaging plane (●).

of state-selected nascent S-atoms. Hence we are able to clearly identify active reaction channels and branching ratios, and to determine the product state distribution for both the atomic and molecular fragment.

Experimental Section

The experimental apparatus used in this study has been described in detail elsewhere.[18] In brief, a gas sample, containing 5% CS_2 in He or Ar, is expanded into the source vacuum chamber *via* a home-built[19] pulsed-molecular beam operating at 20 Hz. Using a nozzle diameter of 0.8 mm, the stagnation pressure is varied between 0.5 and 2 atm in order to study the effects of cluster formation. A photolysis laser beam generated by frequency doubling the output of an excimer-pumped (Lumonics, HyperX-400 operating with XeCl) pulsed-dye (ELTO 1233, operating with Coumarin 540, Rhodamine 590) laser using a KDP crystal is focused onto the collimated beam of neutrals using a lens with a 20 cm focal length. For the present "one-color" experiment the CS_2 photolysis laser pulse is also used for the REMPI of the nascent S-atom photofragments. The velocity distribution of the S-atom photofragments produces a Doppler energy shift in the resonant transition used for their (2+1)MPI which is larger than the laser bandwidth. Hence it is necessary to tune the laser in order to ensure that all photofragments are ionized with equal probability. The laser power is maintained between 250−400 μJ/pulse in order to minimize space charge effects from excessive ion production in the interaction region. Ions produced are accelerated along the axis of the machine toward a home-build position-sensitive ion-imaging detector located approximately 45 cm from the interaction region. Ion images are recorded using a charge-coupled-device (CCD) video camera (COHU). Background images are obtained by tuning the photoionizing laser off-resonance and are subtracted from the ion images. All data images are averaged with respect to the symmetry axis (laser polarization direction) and subsequently averaged with respect to the center-of-symmetry (molecular beam position), such as to correct for possible inhomogeneities in the position-sensitive detector or the CCD.

Results

Both ground ($^3P_{2,1,0}$) and electronically excited ($^1D_2$) S-atom photofragments are state selectively detected using (2+1)REMPI *via* the $4^3P_2 \leftarrow {}^3P_{2,1,0}$ and $4^1F \leftarrow {}^1D_2$ transitions which occur at energies 64 893, 64 496, 64 320, 69 399 cm^{-1}, respectively.[20] Shown in Figure 1 a,b are ion images for $S(^1D_2)$ obtained from the photolysis of CS_2 seeded in a molecular beam of He (stagnation pressure ~ 0.5 atm) and Ar (stagnation pressure ~ 0.5 atm) respectively. Although both images are "dumbbell" shaped with most of the intensity appearing along the laser polarization direction, image 1a appears to be substantially larger in diameter than image 1b. A necessary condition for reconstructing the 3D distribution by directly inverting these ion images (projections) is that all processes involved (photodissociation and MPI detection) are cylindrically symmetric with respect to the photolysis laser polarization.[21] To verify this condition in our experiment, the image of $S(^1D_2)$ shown in Figure 1c is obtained by maintaining the laser polarization perpendicular to the detector's surface plane. No evidence of broken symmetry is observed.[22]

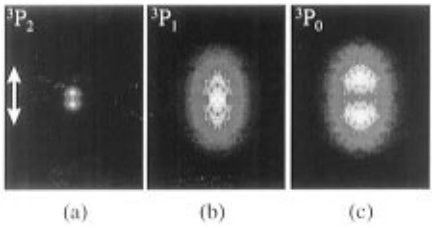

Figure 2. Ion images for the $S(^3P_{2,1,0})$ photofragment following the two-photon excitation of CS_2 seeded in a molecular beam of He, with the laser polarization parallel to the imaging plane (vertical double arrow).

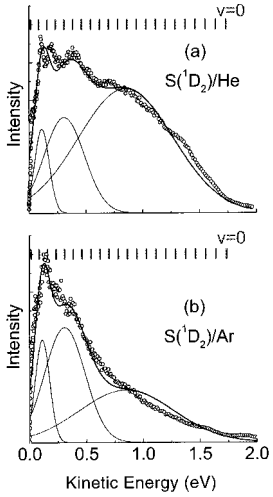

Figure 3. (a) Translational energy distribution for the $S(^1D_2)$ photofragment following the two-photon excitation of CS_2 seeded in a molecular beam of He. (b) Translational energy distribution for the $S(^1D_2)$ photofragment following the two-photon excitation of CS_2 seeded in a molecular beam of Ar. The tic marks indicate the expected S-atom kinetic energies energies corresponding to formation of $CS(X^1\Sigma^+, v, J = 0)$, and the Gaussian curves are simulations corresponding to translational energy distributions of CS_2, $(CS_2)_2$, and $(CS_2)_3$ (see text).

The photofragment images for the $S(^3P_{2,1,0})$ shown in Figure 2 clearly indicate that the S-atom velocity distribution depends strongly on which spin−orbit state is being probed. Specifically, we observe that the $^3P_0$ image is similar in shape to the $^1D_2$ image (Figure 1a), while the $^3P_1$ image is more oval in shape, with nearly uniform intensity throughout its central region. The $^3P_2$ image is markedly different consisting of two very bright lobes in the central region of the image and very little intensity away from the center of the image.

Quantitative scattering information such as translational energy distributions (TED) (Figures 3 and 4) and differential cross sections (DCS) (Figure 5) are obtained from the data images using appropriate image processing described elsewhere.[18,23] The translational energy E_T for the S-atom photofragment is given by the relationship

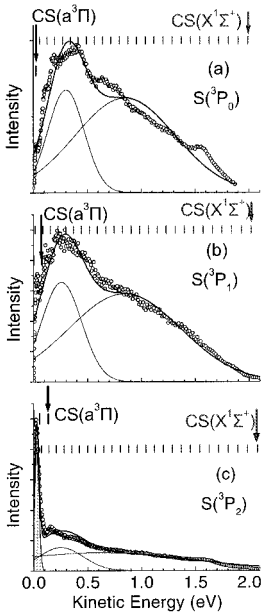

Figure 4. Translational energy distribution for the $S(^3P_{2,1,0})$ photofragments following the two-photon excitation of CS_2 seeded in a molecular beam of He. The tic marks indicate the expected and S-atom kinetic energies corresponding to formation of $CS(X^1\Sigma^+,v,J=0)$ and $CS(a^3\Pi,v,J=0)$, and the Gaussian curves are simulations corresponding to translational energy distributions of CS_2 and $(CS_2)_N$, $N = 2$ and 3 (see text).

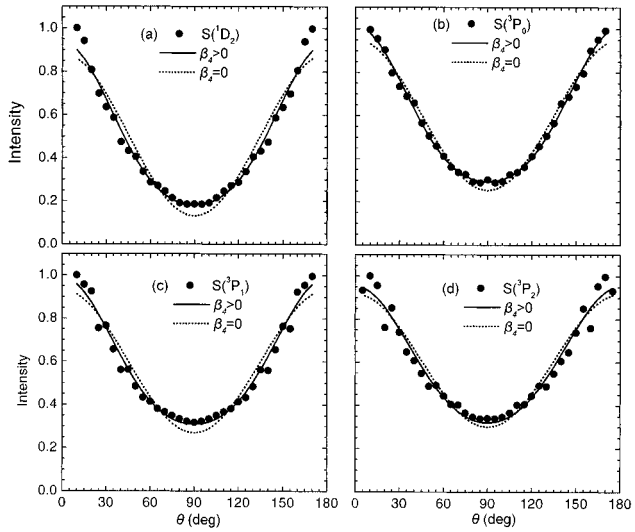

Figure 5. Differential cross sections for the $S(^1D_2,^3P_{2,1,0})$ photofragments following the two-photon excitation of CS_2 seeded in a molecular beam of He, obtained by integrating the outer portion of the ion images: (●) experimental point, (—) simulation with $\beta_4 > 0$, (···), and simulation with $\beta_4 = 0$.

$$E_T = \frac{m(CS)}{m(CS_2)}[2E_{ph} - \Delta G_{v,J}(CS) - \Delta G_e(CS) - \Delta G_e(S) - D_o(CS_2)] \quad (1)$$

where E_{ph} is the photon energy, $D_0(CS_2)$ the dissociation energy of CS_2, $\Delta G_{v,J}(CS)$ and $\Delta G_e(CS)$ are the rovibrational and electronic energies of the CS photofragment, and $\Delta G_e(S)$ the electronic excitation energy of the S atom. Calculated stick spectra indicating the S-atom translational energy corresponding to formation of energetically allowed internal states of $CS[X^1\Sigma^+(v,J=0)]$ and $CS[a^3\Pi(v,J=0)]$ are presented as overlays in each TED plot. Comparison between the experimental TED and the calculated stick spectrum suggests that the CS photofragment is vibrationally very hot, while the TED for both the $S(^3P_2)$ and $S(^3P_1)$ suggest that electronically excited $CS(a^3\Pi)$ is also produced by the photofragmentation process.

The experimental DCS, *i.e.*, the angular distribution of the S-atom photofragment are fit to a functional form $f(\theta)$

$$f(\theta) \sim 1 + \beta_2 P_2(\cos\theta) + \beta_4 P_4(\cos\theta) \quad (2)$$

where $P_2(\cos\theta)$ and $P_4(\cos\theta)$ are the second- and fourth-order Legendre polynomials, β_2 and β_4 anisotropy parameters, and θ is the angle between the laser polarization axis and the velocity vector of the photofragment.[16,24] The β_2 and β_4 values determined are summarized in Table 1.

Discussion

This report deals with the photodissociation dynamics of CS_2 at 8.6 and 8.0 eV following the two-photon excitation at ~288 and ~308 nm, respectively. These excitation energies coincide with the resonant transitions in the sulfur atom thus enabling us to simultaneously probe the nascent S-atom photofragments using (2+1) REMPI. Hence, the experimental excitation energy depends on which state is being probed and the energetically allowed channels for various probe energies are

$$CS_2 \longrightarrow \begin{cases} \text{(a) } CS[X^1\Sigma^+(v=26)] \\ \text{(b) } CS[a^3\Pi(v=1)] \end{cases} + S(^3P_2) \quad \text{(I)}$$

$$CS_2 \longrightarrow \begin{cases} \text{(a) } CS[X^1\Sigma^+(v=25)] \\ \text{(b) } CS[a^3\Pi(v=0)] \end{cases} + S(^3P_1) \quad \text{(II)}$$

$$CS_2 \longrightarrow \begin{cases} \text{(a) } CS[X^1\Sigma^+(v=24)] \\ \text{(b) } CS[a^3\Pi(v=0)] \end{cases} + S(^3P_0) \quad \text{(III)}$$

$$CS_2 \longrightarrow CS[X^1\Sigma^+(v=21)] + S(^1D_2) \quad \text{(IV)}$$

Identification of each photodissociation channel is achieved *via* the state selective detection of the S atom, while further identification of the internal state distribution of the CS fragment is done by analyzing translational energy distribution.

1. $S(^1D_2)$ Formation. The TED for the S atoms produced by channel IV is shown in Figure 3. This channel is 3 eV exoergic, and eq 1 dictates that the maximum translational energy of the S atoms produced will be 1.73 eV. However, the experimental TED peaks at much lower kinetic energies suggesting that a significant portion of the excess energy is consumed by internal excitation of the CS photofragment.

Although the resolution of our spectrometer[18] ($\Delta E/E \approx 20\%$) does not permit rovibrational structure to be observed, some partially resolved features consistently appear at low kinetic energies. When seeding the CS_2 in Ar, the shape of the TED changes drastically such that very little intensity is observed at S-atom translational energies greater than 0.6 eV. The quenched energy region of the TED does not correspond to hot bands as it is well below the 1.73 eV energetic limit. However, the increased probability of forming clusters associated with a colder expansion, as a result of using a heavier carrier gas, suggests that the photodissociation of clusters such as $(CS_2)_N$ could produce S-atoms with low kinetic energies ($E_T \leq 0.6$ eV). When using He, if the stagnation pressure is increased beyond 1 atm, the ion images become identical to those obtained using Ar as the carrier gas. This suggests that true $(CS_2)_N$ clusters, rather than mixed CS_2Ar_N clusters, are responsible for dependence of the ion images on the source conditions. Hence, we assign the partially resolved features at 0.1 and 0.3 eV to the photofragmentation of $(CS_2)_3$ and $(CS_2)_2$, respectively. Similar effects have been reported by Ng and co-workers[4] in the 193 nm

TABLE 1

state	β_2	β_4	β_i	τ	β_2(TOT)	β_4(TOT)	β[a]
$^1D_2$	1.22(0.05)	0.29(0.05)	2.0(0.5)	1.0(0.3)	0.93 (0.03)	0.22 (0.03)	
					1.02 (0.05)	0	0.88(0.08)
$^3P_0$	0.92(0.02)	0.18(0.02)	1.4(0.5)	1.5(0.3)	0.75(0.04)	0.14(0.04)	
					0.81(0.1)	0	0.54(0.07)
$^3P_1$	0.86(0.04)	0.14(0.04)	0.9(0.4)	1.5(0.3)	0.51(0.08)	0	0.52(0.07)
$^3P_2$	0.80(0.04)	0.10(0.04)	0.6(0.4)	1.5(0.3)	0.52(0.08)	0	0.52(0.07)

[a] From ref 16.

photofragmentation studies of CS_2. This assignment raises some questions concerning the nature of these clusters and their dissociation mechanism. For a sequential process

$$(CS_2)_N \rightarrow S + CS(v)(CS_2)_{N-1} \rightarrow S + CS(v) + (CS_2)_{N-1} \quad (3)$$

eq 1 predicts that the S-atom translational energy distribution for a weakly bonded van der Waals type cluster will peak at translational energies greater than that of the monomer,[25] in contradiction with our observations. Consequently, either the internal energy excitation of the $CS(CS_2)_N$ photofragment is substantially greater than that of the CS fragment of channel IV, or these clusters form real chemical bonds with significant binding energies (~1 eV). Alternatively, assuming the clusters underwent a concerted photofragmentation, *i.e.*, $(CS_2)_N \rightarrow S + CS + (CS_2)_{N-1}$, then if the $(CS_2)_{N-1}$ is merely a spectator to the process, we would expect a translational energy release to be identical to the monomer, decreased only by binding energy of the cluster. This once again implies strong binding in these CS_2 clusters.

As the cluster features are only partially resolved, it is difficult to unambiguously determine the CS product state distribution. Stagnation pressures as low as 500 mbar and gas mixtures of 2% CS_2/He are insufficient to inhibit the cluster formation. Assuming that only the mole fraction of the clusters in the beam are affected by source conditions and that only dimers and trimers are the major "contaminants", we model the experimental TED using three Gaussian functions. From the area of the simulation curves we find that the concentrations of CS_2, $(CS_2)_2$, and $(CS_2)_3$ in our He beam are approximately 70%, 23%, and 7% respectively. The simulation curve for CS_2 peaks at energies corresponding to formation of $CS(X^1\Sigma^+, v = 12)$, which means that only 50% of the available energy appears as translational energy. A classical impulsive model[26,27] predicts that the fraction of the available energy appearing as product vibrational energy for a process $ABC \rightarrow A + BC$ is given by the relationship

$$\frac{\Delta E_v}{E_{AVL}} = \frac{m_A m_C}{(m_A + m_B)(m_B + m_C)} \quad (4)$$

ΔE_v and E_{AVL} are vibrational and available energy respectively. In our case eq 4 yields $\Delta E_v/E_{AVL} = 53\%$, in close agreement with our results. In simulating the TED obtained using Ar carrier gas, the positions and widths of the Gaussian curves are the *identical* to those used in the He analysis and *only their amplitudes* are varied, thus confirming our assumption that only the mole fractions of the clusters in the beam are affected by the source conditions.

Photofragment angular distributions are determined in two ways: First by integrating the entire image, thus producing a distribution described by anisotropy parameters β_2(TOT) and β_4(TOT). Second, by integrating the outer portion of the image in order to exclude contributions from clusters and the resulting distribution is characterized by β_2 and β_4. The latter anisotropy parameter values could be considered as upper limits, as they do not include the contributions from the S atoms with low kinetic energies and generally $|\beta_2|$ decreases as the speed of the photofragment decreases.[28]

The coefficients β_2 and β_4 can be related to the lifetime τ of the dissociative state *via* the relationships[15,24]

$$\beta_2 \approx 2P_2(\cos\chi_f)\frac{70 + 55\beta_i}{70 + 28\beta_i}\frac{1 + \omega^2\tau^2}{1 + 4\omega^2\tau^2} \quad (5)$$

$$\beta_4 \approx 2P_4(\cos\chi_f)\frac{18\beta_i}{35 + 14\beta_i}\frac{1 + \omega^2\tau^2}{1 + 4\omega^2\tau^2}\frac{1 + 9\omega^2\tau^2}{1 + 16\omega^2\tau^2} \quad (6)$$

where $\omega \approx (\pi kT/2I)^{1/2}$ is the angular velocity of the parent molecule, I is the moment of inertia, χ_f is the angle between the internuclear axis and the direction of the transition dipole (for the final state), and β_i the anisotropy parameter for the intermediate state. Solving eqs 5 and 6 we find that

$$\beta_i = \frac{35\beta_4}{36P_4(\cos\chi_f)T - 14\beta_4} \quad (7)$$

where

$$T = \frac{1 + \omega^2\tau^2}{1 + 4\omega^2\tau^2}\frac{1 + 9\omega^2\tau^2}{1 + 16\omega^2\tau^2}$$

and

$$\left(192\beta_4 + 72P_4(\cos\chi_f) - 144\frac{P_4(\cos\chi_f)}{P_2(\cos\chi_f)}\beta_2\right)\omega^4\tau^4 + \left(60\beta_4 + 80P_4(\cos\chi_f) - 52\frac{P_4(\cos\chi_f)}{P_2(\cos\chi_f)}\beta_2\right)\omega^2\tau^2 + \left(3\beta_4 + 8P_4(\cos\chi_f) - 4\frac{P_4(\cos\chi_f)}{P_2(\cos\chi_f)}\beta_2\right) = 0 \quad (8)$$

It is clear from eq 7 that if $\beta_i = 0$, then $\beta_4 = 0$, in other words the angular distribution for the two-photon excitation in this case would be similar to a single-photon excitation. Setting $\beta_i = 0$ is equivalent to stating that following the absorption of the first photon, all orientations of the molecule in the intermediate state are equally probable. This situation can only be achieved if the lifetime of this intermediate state is substantially longer than the rotational period of the molecule, thus providing sufficient amount of time for the molecular orientations to randomize. In light of this argument, as the first photon in this experiment is *nearly resonant* with the stable $^1B_2$ excited electronic state in CS_2(V Band),[29,30] Arikawa and co-workers[16] have suggested that β_4 could be ignored. By setting $\beta_4 = 0$ in eq 2 we find β_2(TOT) = 1.02 ± 0.05 in fair agreement with the previously reported value β_2(TOT) = 0.88 ± 0.07 by Arikawa and co-workers.[16] However, inspection of Figure 5 clearly indicates that inclusion of the β_4 term substantially improves the simulations which implies that the first photon is not quite resonant with a specific transition to the $^1B_2$ state, not

surprising as the absorption intensity for the V Band at this energy is extremely weak.[29,30]

Baker *et al.*[31] and Morgan *et al.*[32] have studied the structure of CS_2 near 69 399 cm^{-1} *via* two-photon and three-photon excitations. Specifically Morgan *et al.*[32] have assigned a broad transition at 69414 cm^{-1} to linear $^3\Pi_g$ Rydberg state, while higher resolution measurements of Baker *et al.*[31] have observed transitions at energies of 69 330 cm^{-1} (peak E) assigned to the $^3\Sigma_g^-$ Rydberg state, 69 369 cm^{-1} (peak F, unassigned), 69 446 cm^{-1} (peak G) assigned to $^1\Pi_g/^1\Delta_g$ Rydberg states, and the origin band (0_0^0) for a transition to a $^1\Sigma_g^+$ Rydberg state has been reported at 69 861 cm^{-1}. Our excitation energy is 69 cm^{-1} higher than the transition energy for the $^3\Sigma_g^-$ state, and it appears to be midway between the partially resolved broad peaks E and G. The positive anisotropy parameter observed in our experiment indicates a parallel transition ($\Sigma \rightarrow \Sigma$), which favors the $^3\Sigma_g^-$ state. Our excitation energy is also 462 cm^{-1} lower than the 0_0^0 transition to the $^1\Sigma_g^+$ state, and it is possible that we are exciting a sequence band in the antisymmetric stretch (3_1^1). This would of course require population in the $v = 1$ antisymmetric stretch of the $X^1\Sigma_g^+$ ground electronic state, which is feasible considering that our source conditions were rather "hot" such as to minimize the cluster formation. In light of the above, a definitive assignment of the excited electronic state at our excitation energy (69 399 cm^{-1}) to the $^3\Sigma_g^-$ and $^1\Sigma_g^+$ Rydberg states identified by Baker *et al.*[31] and Morgan *et al.*[32] in this energy region is not possible. However, we estimate the lifetime of the excited state from eq 8 using the β_2 and β_4 values listed in Table 1. By setting $\chi_f = 0$ a rotational temperature of ~100 K and $r_o(CS) \approx 1.6$ Å[33] then $\omega = 0.9 \times 10^{12}$ s^{-1} and we find that $\tau \approx 1.0 \pm 0.3$ ps. (Increasing χ_f increases β_i, yielding physically insignficant values ($\beta_i \gg 2$), thus lending further support of a linear final state geometry.) In addition, from eq 7 we find that $\beta_i \approx 2P_2(\cos \chi_i) \approx 2$ (see Table 1), hence $\chi_i \approx 0$, *i.e.*, a linear intermediate state which supports our previous speculation that the photon energy is not quite resonant with a transition to the bent $^1B_2$ state. Hence the molecule never attains the bent geometry in the intermediate state but instead maintains the linear structure of the ground state (Born−Oppenheimer approximation).

2. S($^3P_{2,1,0}$) Formation. The TED for the $^3P_2$, $^3P_1$, and $^3P_0$ spin−orbit states of the S-atom photofragment are presented in Figure 4a,b,c respectively. The threshold energy for reaction Ib is 63 996 cm^{-1} and is nearly degenerate with the experimental excitation energy 64 320 cm^{-1} when $^3P_0$ is being probed. Just 500 cm^{-1} above the threshold energy, when probing $^3P_1$, evidence of slight production, CS($a^3\Pi$) is observed. At 900 cm^{-1} above threshold, when probing $^3P_2$, the propensity for CS($a^3\Pi$) production rises sharply and becomes significant, in agreement with previous observations of Black *et al.*[34] We first model the TED for the $^3P_0$ and $^3P_1$ channels from which we determine the relative distributions of dimers and monomers for the CS($X^1\Sigma^+$) channel. As the dimer and trimers contributions are not resolved at these energies, we use two rather than three Gaussian curves and find that the cluster concentration in the beam is 27 ± 6% for both the $^3P_0$ and $^3P_1$ channels, consistent, as expected, with the $^1D_2$ results since the source conditions are identical. We scale the determined cluster/monomer distribution with respect to a Gaussian curve used to model the peak corresponding to the CS($a^3\Pi$) channel, fitting in this manner the observed TED for the $^3P_2$ channel. We find that the TED distributions peak at energies corresponding to formation of CS($X^1\Sigma^+$, $v = 14$), *i.e.*, $\Delta E_v/E_{AVL} \approx 45\%$, once again in agreement with the predictions of the classical impulsive model (eq 8). From the areas of the simulation curves in Figure 4c we determine that the branching ratio CS($a^3\Pi$) + S($^3P_2$)/CS($X^1\Sigma^+$) + S($^3P_2$) at excitation energy 64 893 cm^{-1} is 0.22 ± 0.05.

The angular distribution is determined using the same procedure as for the S($^1D_2$) photofragment. As the size of the image corresponding to formation of CS($a^3\Pi$) is very small we are unable to determine anisotropy parameters for this channel, while once again we note that inclusion of the β_4 term substantially improves the angular distribution simulations. Unlike the S($^1D_2$) results however, when setting $\chi_f = 0$ we find that $\beta_i < 2$, suggesting a bent intermediate state. This is expected since the excitation energies used for probing the triplet sulfur states are very close the absorption maximum of the V band. Specifically we find that β_i takes on values of 1.43, 0.94, and 0.59 for spin−orbit levels $J = 0$, 1, and 2, respectively (see Table 1). Assuming that the transition dipole moment lies along the S−S direction, as the S−C−S angle is 131° for the $^1B_2$ state,[30] $\chi_i = 24.5°$, *i.e.*, the angle between the dipole moment direction and the CS bond) and we expect a limiting value of $\beta_i \approx 2P_2(\cos \chi_i) = 1.48$, in excellent agreement with the value observed when $J = 0$. The decrease in β_i as a function of excitation energy means once again that the *lifetime* of the intermediate state must be increasing, *i.e.*, the transition is getting closer to resonance. Comparing our excitation energies with resonant transitions observed in jet-cooled CS_2 spectrum by Kasahara *et al.*[30] we note that our excitation energies when probing $^3P_2$ and $^3P_1$ correspond to fundamental bands 32V and 28V ($\nu' = 3 \leftarrow \nu'' = 0\Sigma$), respectively, while the excitation energy for $^3P_0$ corresponds to the weak band 26V which has been assigned by Jungen *et al.*[29] to the hot band ($\nu' = 3 \leftarrow \nu'' = 2\Delta$). Assuming that our expansion is sufficiently cold to quench any vibrational excitation, we don't expect any population in $\nu'' = 2$, and consequently the excitation energy in the $^3P_0$ situation is essentially nonresonant, hence the observed limiting value $\beta_i = 1.43$. For $J = 2$ and 1 our excitation energies are −5 and +18 cm^{-1} off the transition energies reported for bands 32V and 28V, respectively, hence we expect β_i to be smaller for the $J = 2$ situation than for $J = 1$, consistent with our observations.

The linear nature of the final state ($\chi_f = 0$) predicted by our data analysis agrees with REMPI studies of CS_2 in this energy region[31,32,35] which have identified the $^1\Delta_u$, $^3\Delta_u$, $^1\Sigma_u^+$, and $^3\Sigma_u^+$ Rydberg states in this energy region. Although two-photon electronic transitions to these *u* states are symmetry forbidden, they become vibronically allowed through the π_u bending mode of CS_2. The above electronic states when coupled to a single quantum of bending will yield a $^{1,3}\Pi_g$ vibronic state. Our positive anisotropy parameters once again favor parallel transitions hence once again a Σ type final state; consequently, a perpendicular transition to a Π_g vibronic state would contradict our observations. However, in a Hund's (c) coupling scheme a $^3\Pi_g$ state would have components 0_g^+,0_g^-,1_g,2_g, and a parallel transition to the 0_g^+ component would be consistent with our observed angular distribution. This makes both the $^3\Delta_u$ and $^3\Sigma_u^+$ Rydberg states suitable candidates for the excited electronic state involved in the photodissociation process . The origin of the transition to the $^3\Sigma_u^+$ state is at 63 050 cm^{-1} and the only vibronic transition to this state has been identified at 63 700 cm^{-1},[32] both excitation energies substantially lower than in our experiment. A vibronic transition to the $^3\Delta_u$ state has been tentatively identified at 64 893 cm^{-1},[35] an energy that matches our excitation energy for the S($^3P_2$) channel. An absorption band also assigned to vibronic transitions to a $^3\Delta_u$ state has also been reported by Baker *et al.*[35] at our excitation energies for the S($^3P_{0,1}$) channels. As our experimental excita-

tion energy varies over a range of 573 cm^{-1} depending on which spin−orbit state of the S atom is being detected and given the complex nature of the CS_2 spectroscopy in this energy region, it is possible that different final states are being probed depending on which $S(^3P_J)$ state is being probed. Hence, although the arguments presented above favor a $^3\Delta_u$ excited state, this is only a tentative assignment. Using eq 8 and the β_2 and β_4 values listed in Table 1we can estimate the lifetime of the final state(s), and find it (them) to be 1.5 ± 0.3 ps, for all $S(^3P_J)$ channels.

Acknowledgment. We thank Dr. S. Couris, Prof. D. Charalambidis, Prof. C. Fotakis, Dr. S. Georgiou, Dr. T. Gougousi, and Dr. Michalis Velegrakis for many enlightening discussions and careful reading of the manuscript. We would also like to thank Prof. D. M. Neumark and the Department of Chemistry at UC Berkeley for loaning us the excimer laser used in this experiment. This work is supported by the General Secretariat for Research and Technology under the program PENED94 and is conducted at the Ultraviolet Laser Facility operating at FORTH-IESL (Human Capital and Mobility, Access to Large Scale Facilities EU program, Contract CHGE-CT92-007).

References and Notes

(1) Rabalais, R. W.; McDonald, J. M.; Scherr, V.; McGlynn, S. P. *Chem. Rev.* **1971**, *71*, 73.
(2) Frey, J. G.; Felder, P. *Chem. Phys.* **1996**, *202*, 397.
(3) Waller, I. M.; Hepburn, J. W. *J. Chem. Phys.* **1987**, *87*, 3261.
(4) Tzeng, W. B.; Yin, H. M.; Leung, W. Y.; Luo, J. Y.; Nourbakhsh, S.; Flesch, G. D.; Ng, C. Y. *J. Chem. Phys.* **1988**, *88*, 1658.
(5) McCrary, V. R.; Lu, R.; Zakheim, D.; Russell, J. A.; Halpern, J. B.; Jackson, W. M. *J. Chem. Phys.* **1985**, *83*, 3481.
(6) Yang, S. C.; Freedman, A.; Kawasaki, M.; Bersohn, R. *J. Chem. Phys.* **1980**, *72*, 4058.
(7) Butler, J. E.; Drozdoski, W. S.; McDonald, J. R. *Chem. Phys.* **1980**, *50*, 413.
(8) Kanamori, H.; Hirota, E. *J. Chem. Phys.* **1987**, *86*, 3901.
(9) Starrs, C.; Jego, M. N.; Mank, A.; Hepburn, J. W. *J. Phys. Chem.* **1992**, *96*, 6526.
(10) Norwood, K.; Nourbakhsh, S.; He, G. Z.; Ng, C. Y. *Chem. Phys. Lett.* **1991**, *184*, 147.
(11) Brewer, P.; Van Veen, N.; Bersohn, R. *Chem. Phys. Lett.* **1982**, *91*, 126.
(12) Fotakis, C.; Zevgolis, D.; Efthimiopoulos, T.; Patsilinakou, E. *Chem. Phys. Lett.* **1984**, *110*, 73. Patsilinakou, E.; Proch, D.; Fotakis, C. *Chem. Phys.* **1991**, *153*, 503.
(13) Hardwick, J. L.; Ono, Y.; Moseley, J. T. *J. Phys. Chem.* **1987**, *91*, 4506. Ono, Y.; Hardwick, J. L. *J. Mol. Spectrosc.* **1986**, *119*, 107.
(14) Sapers, S. P.; Donaldson, D. J. *Chem. Phys. Lett.* **1992**, *198*, 341. Sapers, S. P.; Adraos, N.; Donaldson, D. J. *J. Chem. Phys.* **1991**, *95*, 1738. Sapers, S. P.; Donaldson, D. J. *J. Phys. Chem.* **1990**, *94*, 8918.
(15) Kawasaki, M.; Sato, H.; Kikuchi, T.; Fukuroda, A.; Kobayashi, A.; Arikawa, T. *J. Chem. Phys.* **1987**, *86*, 4425.
(16) Kawasaki, M.; Sato, H.; Kobayashi, A.; Arikawa, T. *Chem. Phys. Lett.* **1988**, *146*, 101.
(17) Chandler, D. W.; Houston, P. L. *J. Chem. Phys.* 1987, *87*, 1445.
(18) Samartzis, P. C.; Sakellariou, I.; Gougousi, T.; Kitsopoulos, T. N. *J. Chem. Phys.* **1997**, *107*, 1.
(19) Proch D.; Trickl, T. *Rev. Sci. Instrum.* **1989**, *60*, 713.
(20) Moore, C. E. *Atomic Energy Levels as Derived from the Analyses of Optical Spectra;* U.S. National Bureau of Standards Cirular 467; U.S. National Bureau of Standards, Government Printing Office: Washington, DC, 1949.
(21) Heck, A. J. R.; Chandler, D. W. *Annu. Rev. Phys. Chem.* **1995**, *46*, 335.
(22) Mo, Y.; Katayanagi, H.; Heaven, M. C.; Suzuki, T. *Phys. Rev. Lett.* **1996**, *77*, *830.*
(23) Chandler, D. W.; Kitsopoulos, T. N.; Buntine, M. A.; Baldwin, D. P.; McKay, R. I.; Heck, A. J. R.; Zare, R. N. *Gas-Phase Chemical Reaction Systems: Experiments and Models 100 Years after Max Bodenstein*. in *Chemical Physics*; Wolfrum, J., Volpp, H.-R., Rannacher, R., Warnatz J., Eds.; Springer Series; Springer: Berlin, Heidelberg, 1996.
(24) Sander, R. K.; Wilson, K. R. *J. Chem. Phys.* **1975**, *63*, 4242.
(25) This assumes that the internal state distribution of the $CS(CS_2)_N$ fragment is similar to that of the CS fragment observed in the monomer photodissociation.
(26) Holdy, K. E.; Klotz, L. C.; Wilson, K. R. *J. Chem. Phys.* **1970**, *52*, 4588.
(27) Mahan, B. H. *J. Chem. Phys.* **1970**, *52*, 5221.
(28) Busch, G. E.; Wilson, K. R. *J. Chem. Phys.* **1972**, *56*, 3638.
(29) Jungen, C.; Malm, D. N.; Merer, A. J. *Can. J. Phys.* **1973**, *51*, 1471.
(30) Kasahara, H.; Mikami, N.; Ito, M.; Iwata, S.; Suzuki, I. *Chem. Phys.* **1984**, *86*, 173.
(31) Baker, J.; Couris, S. *J. Chem. Phys.* **1996**, *105*, 62.
(32) Morgan, R. A.; Baldwin, M. A.; Orr-Ewing, A. J.; Ashfold, M. N. R.; Buma, W. J.; Milan, J. B.; de Lange, C. A. *J. Chem. Phys.* **1996**, *104*, 6117.
(33) Brommer M.; Rosmus, P. *Chem. Phys. Lett.* **1993**, *206*, 540.
(34) Black, G.; Sharpless, R. L.; Slanger, T. G. *J. Chem. Phys.* **1977**, *66*, 2113.
(35) Baker, J.; Couris, S. *J. Chem. Phys.* **1996**, *104*, 6130. *Ibid.* **1995**, *103*, 4847.